Effect of lattice vibrations on magnetic phase transition in bcc iron

Junqi Yin, Markus Eisenbach, and Don M. Nicholson
Oak Ridge National Laboratory, Oak Ridge, Tennessee 37831, USA

Aurelian Rusanu
Joint Institute for Computational Sciences, University of Tennessee, Oak Ridge, Tennessee 37831, USA
(Received 12 July 2012; published 21 December 2012)

The most widely taught example of a magnetic transition is that of Fe at 1043 K. Despite the high temperature most discussions of this transition focus on the magnetic states of a fixed spin lattice with lattice vibrations analyzed separately and simply added. We propose a model of α iron that fully couples spin and displacement degrees of freedom. Results demonstrate a significant departure from models that treat these coordinates independently. The success of the model rests on a first principles calculation of changes in energy with respect to spin configurations on a bcc-iron lattice with displacements. Complete details of environment-dependent exchange interactions that augment the Finnis-Sinclair potential are given and comparisons to measurements are made. We find that coupling has no effect on critical exponents, a small effect on the transition temperature, T_c, and a large effect on the entropy of transformation.

DOI: 10.1103/PhysRevB.86.214423 PACS number(s): 75.10.Hk, 75.40.Cx

The magnetic moment associated iron atoms and the interactions between them (Fig. 1) have a strong dependence on atomic environment, e.g., the interatomic distances which affect the overlap of atomic orbitals.[1] Other local environmental parameters, such as the magnitude and shape of the atomic volume, the number of atoms within the first peak distance of the radial distribution function, etc, also come into play.[2] Due to the magnon-phonon interactions[3] the instantaneous local magnetic moments become very inhomogeneous in the presence of displacements. Figure 1 shows that at T_c the displacements are large, e.g., fluctuations in first nearest neighbor separations exceed the separation of second nearest neighbors, resulting in exchange parameters that depend on the local environment in a complicated manner that cannot be captured by a simple separation dependent interaction. How can this be reconciled with the fact that the classical Heisenberg model already provides a surprisingly reasonable description of the magnetic phase transition in bcc iron,[4] including critical exponents that are close to the measured values?[5–8] In this paper, we take a close look at the role of lattice vibrations in magnetic interactions.

A few studies of the magnon-phonon interaction have been reported.[3,9] In Ref. 3, a model with a distance-dependent exchange parameter $J(r)$ is proposed, where the dependence for both the first- and second-neighbors in bcc iron is found to be linear; hence, there is no contribution from the magnon-phonon coupling. On the other hand, recent studies[10] indicate that $J(r)$ has a rather complex functional form, and an environment-independent pairwise representation is inadequate. The $J(r)$ models fail to capture the longitudinal degrees of freedom in the local magnetic moments,[11] which are an important property of itinerant systems. We introduce local environmental parameters, such as atomic volume, that reflect the change in magnitude of local moments. The environmental parameters go beyond pair interactions in the sense that change in the position of an atom alters the J values for all nearby pairs.

We propose a procedure for obtaining magnetic interactions that differs from Liechtenstein *et al.*;[12] in our procedure a finite deviation at two sites within a paramagnetic configuration (generated by randomly assigning spin directions) is used rather than a perturbation from the ferromagnetic configuration. A configuration was chosen at random from the canonical ensemble ($T \approx T_c$) for a 128 atom system interacting via the Finnis-Sinclair potential.[13] The exchange interaction parameters J_{ij} plotted in Fig. 1 are evaluated by considering four configurations $(\vec{e}_i, \vec{e}_j)$: $(\hat{z}, \hat{z})$, $(-\hat{z}, \hat{z})$, $(\hat{z}, -\hat{z})$, $(-\hat{z}, -\hat{z})$ for a total of $14\,848 = 4 \times 128 \times 58/2$ spin configurations, with corresponding energies E^{ij}, $E^{\bar{i}j}$, $E^{i\bar{j}}$, $E^{\bar{i}\bar{j}}$ as follows:

$$J_{ij} = \tfrac{1}{4}(E^{ij} + E^{\bar{i}\bar{j}} - E^{\bar{i}j} - E^{i\bar{j}}). \tag{1}$$

The energies E^{ij} are calculated using the locally self-consistent multiple scattering (LSMS) first principles method.[14] Note that one of the assumptions of our formula is that the Hamiltonian can be written in terms of pair-spin interactions. To eliminate the effect of the higher order terms, it is important that the energy calculation is performed in a background paramagnetic spin configuration so that the cavity fields for the atoms considered are close to zero.

The J_{ij} of pairs based on the LSMS energy calculations of the heated sample are shown in Fig. 1. For comparison, we also plot the data points of interaction parameters for the first five shells estimated using the layer Korringa-Kohn-Rostoker (KKR) method.[15] The spread of points is partly due to the difference in the local atomic environment resulting from displacements, and partly due to the "background noise" that comes from the residual local cavity field. It is interesting that the first and second nearest neighbor interactions exhibit quite distinctive behavior, and hence should be considered separately.

Our Hamiltonian is

$$H = -\sum_{i<j} J^{\text{eff}}(\vec{e}_i \cdot \vec{e}_j - \langle \vec{e}_i \cdot \vec{e}_j \rangle) + V, \tag{2}$$

where V is the Finnis-Sinclair (FS) interatomic potential for iron, and J^{eff} is the effective exchange interaction obtained

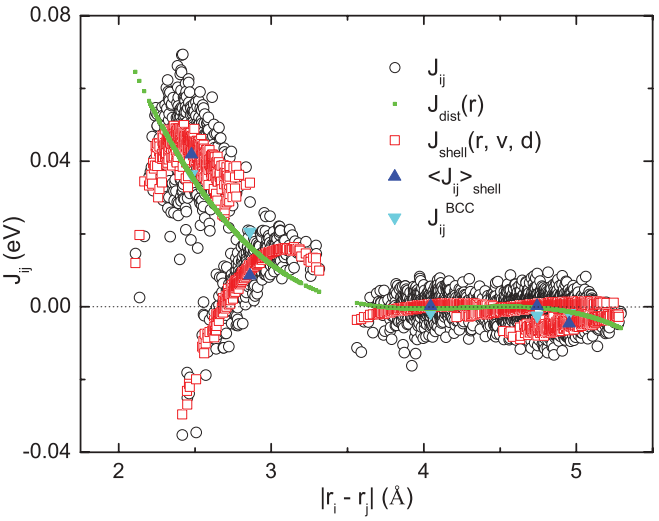

FIG. 1. (Color online) Pair exchange parameters J_{ij} calculated for all pairs (up to fifth nearest neighbor) in a 128 atom cell using the method described in the text (black circle) for a representative configuration (positions and spins) of bcc iron near T_c. The values for each pair are also shown as approximated by a fit to a function of separation, $J_{\rm dist}(r)$ (green dots), and as approximated by the shell dependent function described in the text, $J_{\rm shell}(r,v,d)$ (red squares). The averages within a shell of the exchange interactions, $\langle J_{ij}\rangle_{\rm shell}$, are shown as blue up triangles. Five data points of $J_{ij}^{\rm bcc}$ for perfect bcc from Ref. 15 are plotted as cyan down triangles.

from the first principle calculations. To obtain the same average energy as in the FS potential, we correct the double counting of the ferromagnetic energy by subtracting the spin-spin correlation, which is determined self-consistently. Models of J are compared to Eq. (1) in Fig. 1. We consider first a simple separation-dependent model. The linear regression procedure indicates that the first three orders of the separation ($r = |\vec{r}_i - \vec{r}_j|$, in units of angstroms) are statistically significant. Therefore, we obtain $J_{\rm dist}(r)$ (in units of eV):

$$J_{\rm dist}(r) = 0.519\,057\,5 - 0.367\,938\,8r + 0.086\,530\,5r^2 - 0.006\,755\,2r^3. \quad (3)$$

The independently obtained J values for the perfect crystal[15] are also described by this fitted curve, but it obviously cannot explain the rich behavior of each individual shell. After investigating several parametrizations for characterizing the local atomic environment, we propose $J_{\rm shell}(r,v,d)$:

$$\begin{aligned} J_1^{\rm eff} &= -6.907\,147\,5 + 8.194\,083\,2r \\ &\quad - 3.2248719r^2 + 4.2085021\times10^{-1}r^3 \\ &\quad -4.6127027\times10^{-4}d^2 + 2.1663578\times10^{-3}v, \\ J_2^{\rm eff} &= -1.2902636 + 7.1554984\times10^{-1}r \\ &\quad - 9.3939101\times10^{-2}r^2 + 1.7280909\times10^{-2}v \\ &\quad - 5.7021238\times10^{-3}rv, \\ J_3^{\rm eff} &= -1.5229965\times10^{-1} + 7.2330118\times10^{-2}r \\ &\quad - 8.5256004\times10^{-3}r^2 - 2.4695955\times10^{-5}d^2, \\ J_4^{\rm eff} &= -1.1312616\times10^{-1} + 4.000450\times10^{-2}r \\ &\quad - 3.8278464\times10^{-3}r^2 + 4.3302468\times10^{-4}v \\ &\quad - 2.1941118\times10^{-5}d^2, \end{aligned}$$

$$\begin{aligned} J_5^{\rm eff} &= 4.2015751\times10^{-1} - 7.7863035\times10^{-2}r \\ &\quad - 1.9727826\times10^{-2}v + 3.6452839\times10^{-3}rv, \end{aligned} \quad (4)$$

where $v = v_i + v_j$ is the volume of the Voronoi polyhedra of atoms i and j, and $d = d_i + d_j$ measures the local displacement that relates to the shape of the volume. We define $d_i = \sum_{k\in{\rm nn}(i)} |\vec{p}_k - \vec{p}_k^{\,0}|$ where $\vec{p}_k = \vec{r}_k - \vec{r}_i$ and $\vec{p}_k^{\,0} = \vec{r}_k^{\,0} - \vec{r}_i^{\,0}$. [$\vec{r}_k^{\,0}$ is the corresponding distance vector for the perfect crystal with the lattice constant 2.86Å and nn(i) stands for a set of the nearest-neighbor of atom i.] We exhaust the combination of parameters and keep terms that are significant in statistical tests. To obtain a harmonic energy, only quadratic terms of d are used. Since the intermediate environment may become important for the long distance shell, the fit for the third and fourth shells are not quite as good.

Parallel tempering Monte Carlo simulations[17] are applied with a simulation temperature-set chosen as a geometric series. Since the system has a nondiverging specific heat ($\alpha\langle 0$), the acceptance rate for swapping neighboring replicas is almost constant. Typically, one Monte Carlo step consists of a Metropolis single spin flip and a trial displacement move for every atom. The spin correlation term is updated every step, and the swapping of neighboring replica is attempted every 10 steps. The trial displacement length and the range of simulation temperatures are chosen such that the acceptance rate is above 20%.

In Fig. 2, we plot the specific heats for two treatments: (1) atoms displaced from perfect lattice positions, and (2) atoms frozen at perfect lattice positions. For case 1, we show results for our two exchange expressions [$J_{\rm dist}(r)$ and $J_{\rm shell}(r,v,d)$]. For case 2, we show results where we have averaged the exchange parameters used for case 1 over each shell [$\langle J_{\rm dist}(r)\rangle_{\rm shell}$ and $\langle J_{ij}\rangle_{\rm shell}$]; we add $3k_B$ to independently include the phonon specific heats. Case 2 therefore includes, on average, the change in the exchange interactions due to fluctuations in position but neglects the correlation between

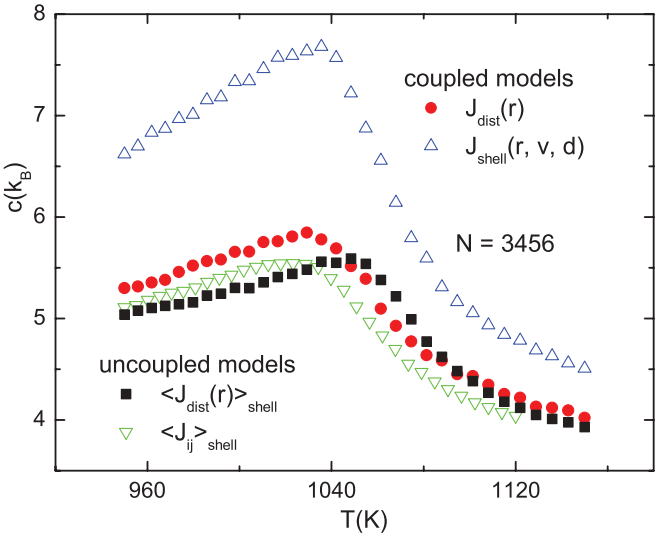

FIG. 2. (Color online) Specific heats for a 12 × 12 × 12 supercell with [$J_{\rm dist}(r)$ and $J_{\rm shell}(r,v,d)$] and without [$\langle J_{\rm dist}(r)\rangle_{\rm shell}$ and $\langle J_{ij}\rangle_{\rm shell}$; each added $3k_B$ for comparisons] coupling between spins and displacements.

spins and displacements. The disorder associated with lattice vibration pushes the specific heat peak calculated with $J_{\rm dist}(r)$ down by 20 K relative to that of $\langle J_{\rm dist}(r)\rangle_{\rm shell}$. The peak position of $J_{\rm dist}(r)$ is close to that of model $\langle J_{ij}\rangle_{\rm shell}$ which averages over the J values of displaced atoms. The curve of $J_{\rm dist}(r)$ is similar in shape and magnitude with those of model $\langle J_{ij}\rangle_{\rm shell}$ and $\langle J_{\rm dist}(r)\rangle_{\rm shell}$, which signals a weak magnon-phonon coupling. Interestingly the $J_{\rm shell}(r,v,d)$ model where we take into account the local atomic environment has a more pronounced specific heat peak that falls at a temperature several degrees higher than that of $J_{\rm dist}(r)$, indicating that strengthened interactions result from magnon-phonon coupling.[3]

Similar effects can be seen in magnetization, as shown in Fig. 3. The curve shape for the $J_{\rm shell}(r,v,d)$ model is distinct from the other three models. It signals a stronger transition at a temperature between that of $\langle J_{ij}\rangle_{\rm shell}$ and $\langle J_{\rm dist}(r)\rangle_{\rm shell}$, and provides a larger magnetization near the transition. Following finite-size scaling analyses of the susceptibility and fourth order cumulants of the magnetization, we determine the transition temperatures for $\langle J_{\rm dist}(r)\rangle_{\rm shell}$, $\langle J_{ij}\rangle_{\rm shell}$, $J_{\rm dist}(r)$, and $J_{\rm shell}(r,v,d)$ to be 1050(4), 1027(2), 1034(2), and 1045(2) K. The T_c of our full model agrees with the measured Curie temperature.

To compare our specific heat with the experimental data,[7,17] we apply a scaling scheme[18] such that the corresponding quantum specific heat can be calculated from the classical one. In Fig. 4, the original and rescaled specific heats of the $J_{\rm shell}(r,v,d)$ model are plotted, along with that of the $\langle J_{ij}\rangle_{\rm shell}$ model. The marked region between the two scaled curves is the contribution from the spin-lattice coupling, which is significant near the phase transition. Essentially, our model agrees with the experiment from 400 K to T_c. Since FS is a classical model, the zero temperature limit goes to 3 instead of 0. We attribute the discrepancy at high temperatures to the fact that the FS potential does not reproduce the structural transition of α to γ. Due to the lack of constant volume experimental data around T_c (1010–1080 K), constant pressure data are shown. We mention that the $J_{\rm shell}(r,v,d)$ model in the NPT ensemble provides a T_c about 50 K higher than the Curie temperature although the specific heat curve is similar to the constant volume result in shape and magnitude.

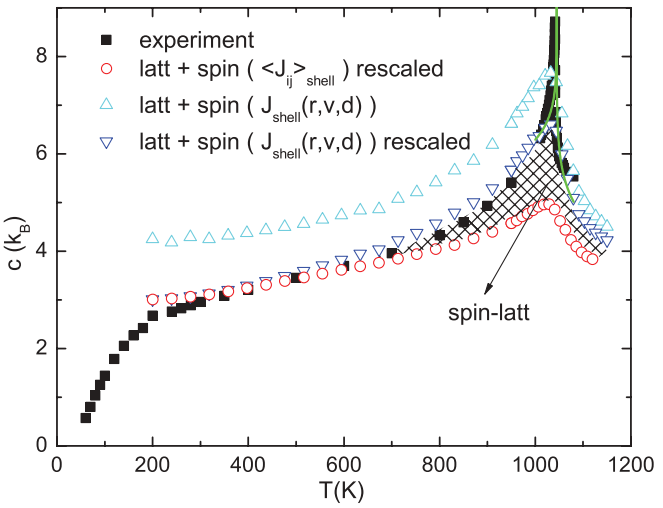

FIG. 4. (Color online) Comparison of specific heat data for a 12 × 12 × 12 supercell for the $J_{\rm shell}(r,v,d)$ model (original and rescaled) and the $\langle J_{ij}\rangle_{\rm shell}$ model (rescaled) with experimental results.[7,17] The solid curve shows the extrapolated infinite size behavior.

In Fig. 5, the magnetization data of $J_{\rm shell}(r,v,d)$ and $\langle J_{ij}\rangle_{\rm shell}$ are compared with the experimental results.[19] The agreement is not as good for temperatures slightly away from the T_c, although it still outperforms the other three models. We suspect that the paramagnetic background in LSMS calculations of J values contributes to the underestimation of the magnetization in the ferromagnetic states, where effective many site interactions are becoming more important.

According to the universality class theory, the underlying microscopic properties, such as the background phonon-phonon interaction, should not affect the critical behavior of

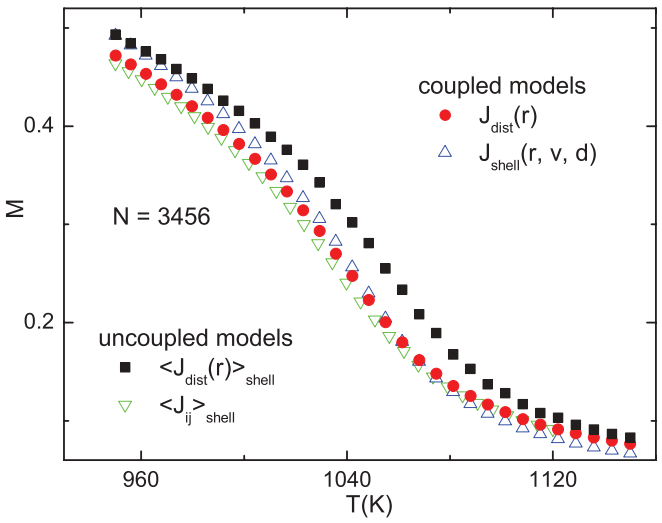

FIG. 3. (Color online) Magnetization for a 12 × 12 × 12 supercell with [$J_{\rm dist}(r)$ and $J_{\rm shell}(r,v,d)$] and without [$\langle J_{\rm dist}(r)\rangle_{\rm shell}$ and $\langle J_{ij}\rangle_{\rm shell}$] coupling between spins and displacements.

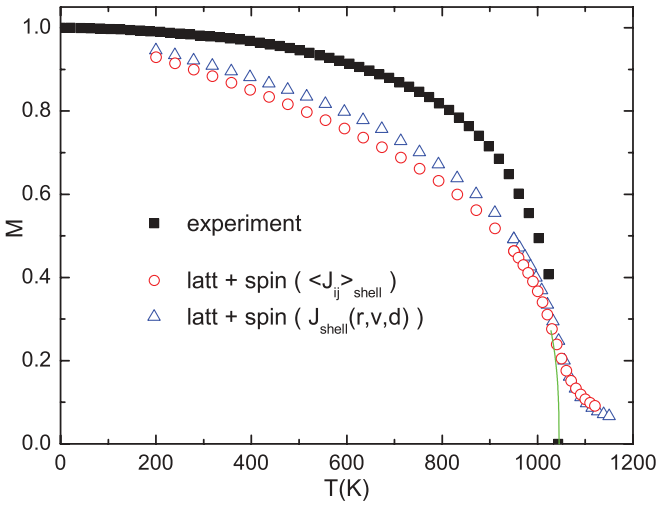

FIG. 5. (Color online) Comparison of magnetization data for a 12 × 12 × 12 supercell for the $J_{\rm shell}(r,v,d)$ model and the $\langle J_{ij}\rangle_{\rm shell}$ model with experimental results.[19] The solid curve shows the extrapolated infinite size behavior.

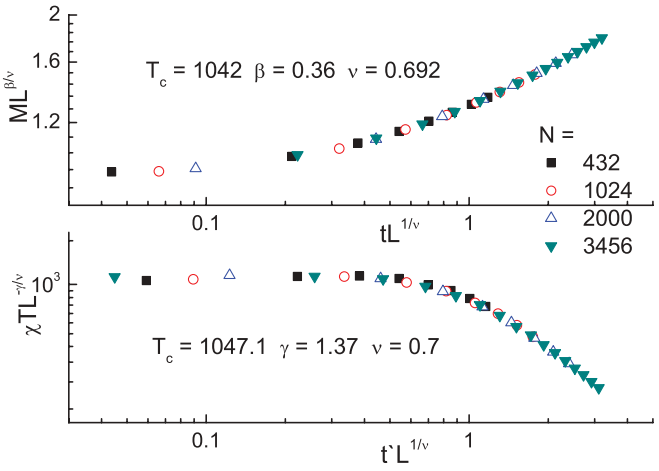

FIG. 6. (Color online) Finite-size scaling plots of magnetization and its susceptibility for the $J_{\text{shell}}(r,v,d)$ model. $t = |1 - \frac{T}{Tc}|$ and $t' = |1 - \frac{T_c}{T}|$.

the system. As it is not obvious whether critical exponents are changed by magnon-phonon interactions, we perform data collapsing for the magnetization and its susceptibility following the finite-size scaling forms $M = L^{-\frac{\beta}{\nu}}\overline{X}(tL^{\frac{1}{\nu}})$ and $\chi T = L^{\frac{\gamma}{\nu}}\overline{Y}(tL^{\frac{1}{\nu}})$, respectively ($t = |1 - \frac{T}{T_c}|$, and $\overline{X}$ and $\overline{Y}$ are unknown universal functions). As shown in Fig. 6, our calculated $\nu = 0.696(4)$, $\beta = 0.360(5)$, and $\gamma = 1.37(2)$ are consistent with both Heisenberg universality [$\alpha = -0.118(11)$, $\beta = 0.3669(32)$, $\gamma = 1.385(10)$ (Ref. 6)] and experimental values [$\alpha = -0.12(1)$ (Ref. 7), $\beta = 0.363(4)$ (Ref. 8), $\gamma = 1.33(2)$ (Ref. 8)].

In conclusion, we proposed a procedure to extract exchange interactions from first principle calculations, and built models that include the effect of lattice vibrations. It is shown that in addition to the interatomic distance, local atomic environmental parameters, such as shell number, atomic volume, etc, play a crucial role in describing the correct magnon-phonon interaction. For bcc iron, our $J_{\text{shell}}(r,v,d)$ model works surprisingly well, when compared to experimental results.

Work is sponsored by the US Department of Energy, Office of Basic Energy Sciences, Materials Sciences and Engineering Division (M.E., D.M.N., for spin-spin coupling), by the "Center for Defect Physics," an Energy Frontier Research Center (A.R., D.M.N., for spin-lattice coupling), and by the Department of Energy, Office of Advanced Scientific Computing Research (J.Y.). This research used resources of the Oak Ridge Leadership Computing Facility at the ORNL, which is supported by the Office of Science of the U.S. Department of Energy under Contract No. DE-AC05-00OR22725.

[1] M. Shimizu, Rep. Prog. Phys. **44**, 329 (1981).
[2] R. F. Sabiryanov, S. K. Bose, and O. N. Mryasov, Phys. Rev. B **51**, 8958 (1995).
[3] R. F. Sabiryanov and S. S. Jaswal, Phys. Rev. Lett. **83**, 2062 (1999).
[4] N. M. Rosengaard and B. Johansson, Phys. Rev. B **55**, 14975 (1997); M. Pajda, J. Kudrnovsky, I. Turek, V. Drchal, and P. Bruno, *ibid.* **64**, 174402 (2001); F. Körmann, A. Dick, B. Grabowski, B. Hallstedt, T. Hickel, and J. Neugebauer, *ibid.* **78**, 033102 (2008).
[5] V. Heine, A. I. Liechtenstein, and O. N. Mryasov, Europhys. Lett. **12**, 545 (1990); A. V. Ruban, S. Khmelevskyi, P. Mohn, and B. Johansson, Phys. Rev. B **75**, 054402 (2007).
[6] K. Chen, A. M. Ferrenberg, and D. P. Landau, Phys. Rev. B **48**, 3249 (1993).
[7] L. W. Shacklette, Phys. Rev. B **9**, 3789 (1974).
[8] N. Stüsser, M. Th. Rekveldt, and T. Spruijt, Phys. Rev. B **31**, 5905 (1985).
[9] K. P. Sinha and U. N. Upadhyaya, Phys. Rev. **127**, 432 (1962); E. Pytte, Ann. Phys. (NY) **32**, 377 (1965); D. J. Kim and I. Yoshida, Phys. Rev. B **52**, 6588 (1995); W. Zhang, J. Magn. Magn. Mat. **323**, 2206 (2011).
[10] S. Morán, C. Ederer, and M. Fähnle, Phys. Rev. B **67**, 012407 (2003); H. Wang, P. W. Ma, and C. H. Woo, *ibid.* **82**, 144304 (2010).
[11] F. Dietermann, L. M. Sandratskii, and M. Fähnle, J. Magn. Magn. Mat. **324**, 2693 (2012).
[12] A. I. Liechtenstein, M. I. Katsnelson, V. P. Antropov, and V. A. Gubanov, J. Magn. Magn. Mater. **67**, 65 (1987).
[13] M. W. Finnis and J. E. Sinclair, Phil. Mag. A **50**, 45 (1984); **53**, 161 (1986).
[14] M. Eisenbach, D. M. Nicholson, A. Rusanu, and G. Brown, J. Appl. Phys. **109**, 07E138 (2011).
[15] X. Tao, D. P. Landau, T. C. Schulthess, and G. M. Stocks, Phys. Rev. Lett. **95**, 087207 (2005).
[16] R. H. Swendsen and J. S. Wang, Phys. Rev. Lett. **57**, 2607 (1986).
[17] G. K. White and M. L. Minges, Int. J. Thermophys. **18**, 1269 (1997).
[18] F. Körmann, A. Dick, T. Hickel, and J. Neugebauer, Phys. Rev. B **81**, 134425 (2010).
[19] J. Crangle and G. M. Goodman, Proc. R. Soc. London A **321**, 477 (1971).